HEFAT2012
9th International Conference on Heat Transfer, Fluid Mechanics and Thermodynamics
16 – 18 July 2012
Malta

SYNTHETIC JETS FOR ELECTRONICS COOLING APPLICATIONS

M. Barış Doğruöz[1] and Mehmet Arik[2]

[1]Amobea Technologies Inc.
11809 La Barzola Bend
Austin, TX, 78738 USA

[2]Ozyegin University
Faculty of Engineering
Department of Mechanical Engineering
Cekmekoy, Istanbul, Turkey
E-mail: mehmet.arik@ozyegin.edu.tr

ABSTRACT

Compact, high functionality electronics resulted in high performance computing. These innovations lead to smaller electronic systems with higher heat fluxes than ever. However, thermal real estate has kept the same or even smaller for posing challenges to thermal scientists. Novel cooling techniques have been of interest to solve the demand. One of these technologies operates with microfludics principle creating vortex rings called *synthetic jets*. These jets are simply meso-scale devices operating at zero-net-mass-flux principle by ingesting and ejecting high velocity working fluid from a single opening. The ingestion/ejection produces periodic jet streams, which may have local velocities over 50 m/s. Based on the published literature, these jets can enhance the heat transfer in both natural and forced convection environments significantly. Recognizing the heat transfer physics over surfaces require a fundamental understanding of the flow physics caused by pulsating coolant flow. A computational study has been performed to understand the flow physics of a small scale synthetic jet. A second-order temporal implicit scheme was used for the unsteady terms to avoid stability issues. No secondary peaks are observed on the surface profiles, and the vortices created at the nozzle exit seem to have no effect on the surface profiles.

INTRODUCTION

While high flux cooling problems are solved with liquid cooling methods, air cooling is still the method of choice for a vast majority of applications. A number of innovative air cooling techniques for low-cost, compact and reliable systems have been considered [1,2]. Air-cooling remains the primary choice of engineers for electronics cooling due to its availability and low cost. The demand for more powerful cooling systems, however, has led scientists to look for unconventional methods that further expand the limits of natural air cooling. One of these methods is the use of synthetic jets in passively or actively cooled electronic systems. The present study investigates meso-scale, i.e. in the order of mm. to cm. size, devices. Synthetic jets are zero-net-mass-flux devices because they intake and eject high velocity working fluid from a single opening. They do, however, have a net momentum-flux. The schematic of a synthetic jet, used in this study, and its operation is shown in Figure 1. A synthetic jet is shown to comprise two circular disk-shaped piezoelectric actuators, bonded together with an elastomeric material applied along the entire perimeter, except for a small "orifice" region. The disks are then energized with an alternating power source to actuate at a certain frequency range (i.e. the range is from 100 to 600 Hz for the present study) to alternately intake and expel air through the orifice. The lower frequency limit represents the experimentally found lowest operating frequency at which the jets start to move enough air to improve heat transfer. The present synthetic jets have a fundamental frequency of around 600 Hz, where the disk displacement and the exit velocity reach their peak values. They are capable of producing periodic jet streams with peak velocities in excess of 20 times the air velocities caused by comparable size conventional fans [3,4]. Any further increase in the frequency results in reduced cooling efficiency and increased power consumption. Operationally, the overall flow-rate of air exiting the synthetic jets is controlled by the driving frequency and the applied voltage across the piezo-electric disks. By suitably changing these parameters, air flows with a range of Reynolds numbers can be obtained.

Synthetic jets have been extensively investigated from the standpoint of flow control [5] and promoting turbulence in

boundary layers [6]. In the past decade, researchers have started to focus on the implementation of such "zero mass but significant positive momentum flux" devices in heat transfer applications to enhance heat transfer in both natural and forced air convection cooled systems [7]. In the case of heat transfer applications, the cooling process can either be facilitated by direct impingement of vortex-dipoles on heated surfaces [8], or via employing the jets to enhance the performance of existing cooling systems [9]. These active cooling devices are particularly well suited for small-scale electronics, such as printed circuit board components, where natural convection is not sufficient and other cooling devices, such as fans, are not practical due to space limitations.

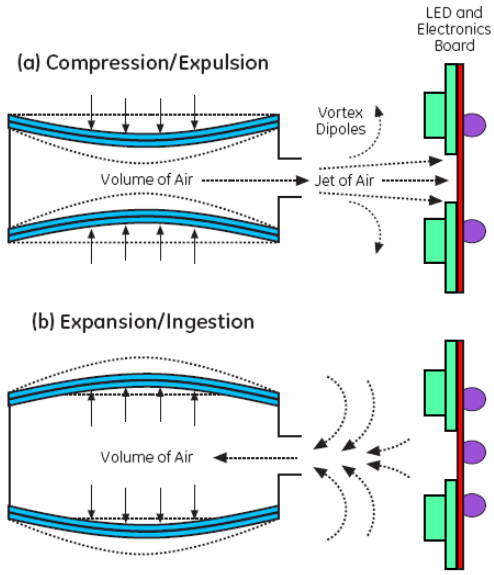

Figure 1 Typical operation of a synthetic jet; synthetic jets shown from top [19].

Use of synthetic jets in heat transfer applications dates back to early 1980s. Gutmark *et al.* [10] presented the first heat transfer data on using synthetic jets for both natural convection and forced convection. The results revealed that vortex induced flow increases the overall heat-transfer coefficient by a factor of four. Later, Yassour *et al.* [11] published their study on synthetic jet augmented heat transfer, where they used loudspeakers as synthetic jet actuators, and found four times enhancement in heat transfer over natural convection. Later, in the late 90's, synthetic jet based acoustic resonators were studied for heat transfer enhancement of microelectronics [7]. Thermal management of a cell phone by using synthetic jet technology was presented by Minichielo *et al.* [12]. They reported a heat transfer enhancement of up to four times compared to natural convection. Utturkar *et al.* [13] further showed that synthetic jets could provide up to a 15-fold enhancement in the local heat transfer coefficient on a square surface in vertical orientation when compared to natural air convection. An experimental investigation of synthetic jet devices to observe the impingement heat transfer over a small heater surface area was studied by Garg *et al.* [14]. They reported a maximum heat transfer augmentation of ten times over natural convection from a vertical surface and further observed that the jet effectiveness strongly depended on the axial distance from the orifice to the heat source and the jet driving frequency. The effects of jet impingement angle and proximity to the heat source on heat transfer were presented in [15]. A 30% reduction in the heat transfer enhancement was observed when the impingement angle was increased from 0° to 90°.

Understanding the fluid structure interaction is very important to predict the synthetic jet cooling performance, noise and power consumption. However, there is very limited data on the complex physics of fluid structure interaction for synthetic jets. Seeley *et al.* [16] developed an analytical model based on Helmholtz resonators to capture the coupled structural dynamics, acoustic and heat transfer physics of synthetic jets. The underlying physics that govern the jet structural and thermal performances were investigated and trade-off studies were performed. In a more recent study [17], acoustic and thermal performance of high frequency synthetic jets and a number of noise abatement strategies were studied. A detailed discussion of the energy efficiency, cooling performance and acoustic issues was given elsewhere [9].

Recently, a study on the cooling effect of a meso scale synthetic jet compared to a steady jet was presented by Arık *et al.* [18]. It is found that synthetic jets can provide more than 20% of cooling than that of a steady impinging jet over vertical surfaces. It is also shown that vortex generated synthetic jet cooling is capable of providing much higher performance than a comparable steady jet for the same jet exit velocity and orifice size.

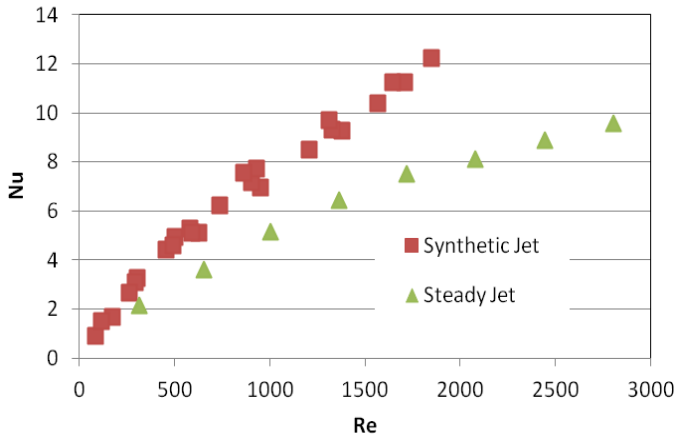

Figure 2 Comparison of a synthetic jet over a steady impinging jet: *Nu* profiles at various *Re* for H/D_h=10 [18].

While synthetic jet cooling has been shown to be an effective method for certain applications in the literature, its fundamental cooling mechanism is not understood well and, therefore is of interest for the current study. Target plate surface profiles and vortex map of a synthetic jet are determined from an unsteady two-dimensional computational analysis. Based on these findings, pertaining discussions are included below.

NOMENCLATURE

A	[m^2]	Area
c_f	[-]	Skin friction coefficient
c_p	[-]	Pressure coefficient
D_h	[m]	Hydraulic diameter
f	[s^{-1}]	Frequency
h	[W/m^2K]	Heat transfer coefficient
H	[m]	Nozzle to target plate height
k	[m^2/s^2]	Turbulence kinetic energy
m	[kg]	Mass
Nu	[-]	Nusselt number=hD_h/κ
P	[Pa]	Pressure
Re	[-]	Reynolds number
t	[s]	Time
T	[K]	Temperature
u	[m/s]	Velocity
x	[m]	Streamwise direction
y	[m]	Wall-normal direction
W	[m]	Nozzle width

Special characters

φ	[rad/deg]	Phase angle
κ	[W/m.K]	Thermal conductivity
ζ	[s]	Period
μ	[Pa.s]	Molecular viscosity
ρ	[kg/m^3]	Mass density

Subscripts

imp	Impinging
h	Hydraulic
j	Jet
syn	Synthetic
w	Wall

COMPUTATIONAL STUDY

In this study, the flow and temperature fields created by a synthetic jet emanated from a rectangular shape nozzle are of interest. As the aspect ratio for the rectangular nozzle is 8:1, the jet can be treated as a two-dimensional jet (note that for an impinging jet, minimum aspect ratio to obtain two-dimensionality is about 6:1).

The computational domain with the boundary conditions is depicted in Figure 3. As can be seen, the computational domain has a length of 32 nozzle widths extending from $-16W \leq x \leq +16W$ in the streamwise direction. The wall-normal direction extends from $y = 0$ (target plate) to $y = H$ (nozzle-exit). A 25 mm x 25 mm strip heater is mimicked with a heated line wall extending to 12.5 nozzle width on the each side of the jet symmetry line. The section between $12.5W$ and $16.0W$ on the target plate is adiabatic. The size of the computational domain in the streamwise direction is chosen such that there is no circulation at the vertical boundaries on each side, therefore these boundaries are taken as zero-pressure boundaries. The synthetic jet is an unconfined jet, i.e. there is no confinement plate at $y = H$ and these boundaries are also treated as zero-pressure boundaries. The time-dependent velocity at the nozzle-exit is a function of sine wave and shown as follows:

$$u(t) = u_j.\sin(2.\pi.f.t) = u_j.\sin\left(2.\pi.\frac{t}{\zeta}\right) \qquad [1]$$

where u_j = 10 m/s, f = 600 Hz and $\zeta = 1.667.10^{-3}$ s. Initially, the temperature at the nozzle-exit ($T(x,0)$) is equal to the ambient temperature of 20°C, where a constant temperature boundary condition is assumed on the heated wall, T_w = 80°C.

A structured rectangular computational grid is generated with necessary refinements in the vicinity of the target plate and the nozzle (see Figure 3). Grid sensitivity of the model is also checked so that the computational results do not vary with further refinements on the grid. The selected grid size is 118 x 48 in x and y directions, respectively. For the spatial discretization, second-order upwind schemes are used to determine the momentum and thermal fields. SIMPLE algorithm for pressure-velocity coupling and k-ε turbulence model with standard wall functions are used in the computations. For the temporal discretization, a second-order implicit scheme is used. Radiation between the heated wall and its surroundings is not taken into account.

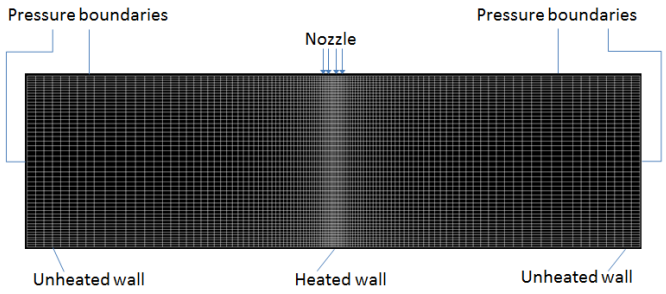

Figure 3 Computational domain, grid and boundary conditions.

RESULTS AND DISCUSSIONS

Prior to showing the synthetic jet results, the authors would like to include a paragraph describing how to determine the Reynolds number for a synthetic jet. As synthetic jets operate with zero mass-flux principle, the time averaged mean velocity at the nozzle-exit is zero. However, in order to make fair comparisons between a synthetic jet and its impinging jet counterpart, the authors suggest that both of the Reynolds number should be written based on the mass ejected from the nozzle. Therefore, in a full period, the mass ejected from the nozzle for a synthetic and impinging jet is written as follows:

$$\int_{m1}^{m2} dm = \int_{n\zeta}^{n\zeta+2\pi} \rho A u(t)\, dt \qquad [2]$$

where A is the area of the nozzle exit. If the synthetic jet operates on a sine wave, and the velocity is spatially invariant at the nozzle-exit, the ratio of the mass ejected by a synthetic jet in a full period to its impinging jet counterpart in the same time interval is:

$$\frac{m_{syn,j}}{m_{imp,j}} = \frac{\cos(2.\pi.f.t))_{n\zeta+1/2f}^{n\zeta}}{\frac{2.\pi.f}{1}} = \frac{1}{\pi} \qquad [3]$$

Therefore, Reynolds number for a synthetic jet can be written as:

$$Re_j = \frac{\rho u_j D_h}{\pi \mu} \quad [4]$$

Wall profiles and vorticity field

Figure 4 shows the non-dimensional pressure profiles of a synthetic jet on the target plate at various times (phase angles) for Re_j=211 and H/D_h=5 (H/W=8.89). The non-dimensional pressure coefficient, c_p is defined as follows:

$$c_p = \frac{P}{0.5.\rho.u_j^2} \quad [5]$$

Sub-ambient pressure values are seen towards the end of injection period, i.e. after about φ=150°. Sub-ambient pressure values continue to exist until the later stages of the suction and disappear at the beginning of the injection period (at φ=0°). If there are no sub-ambient values, the profile is of Gaussian shape.

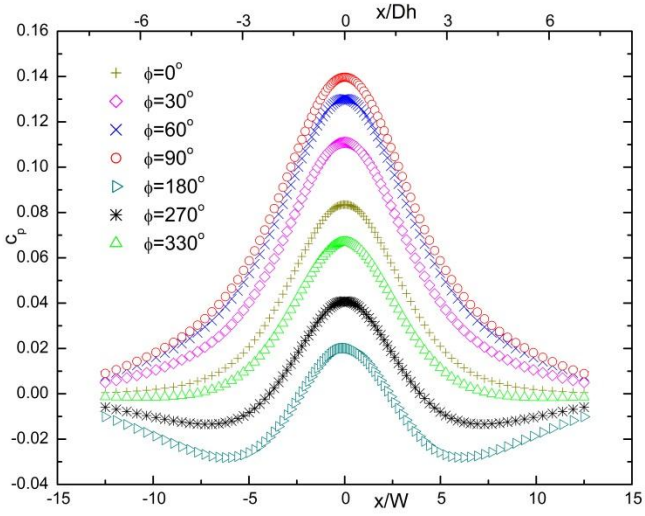

Figure 4 Pressure distribution on the target plate at various phase angles (times), Re_j = 211 and H/D_h = 5 (H/W = 8.89).

It is worth noting that the frequency of the synthetic jet is high enough that the maximum pressure coefficient value, which is obtained at the jet the centreline at any time, never reaches the value that its impinging jet counterpart does. It can be argued that for a synthetic jet, the velocity profile is time dependent at the nozzle-exit and the mass flow rate reaches its maximum at φ=90° where an impinging jet sustains that profile continuously, however the maximum c_p value (at the stagnation point) obtained even at φ=90° is substantially lower than that of the corresponding impinging jet, i.e. 0.14 for a synthetic jet at Re_j=211 and 0.7 for its impinging jet counterpart. In addition, the pressure distribution has a higher half-width (the location where the static pressure is half of the maximum (stagnation) pressure) compared to the corresponding impinging jet, i.e. its half width (≈4W (2.25D_h)) is considerably higher than that of a two-dimensional impinging jet (≈D_h). It should also be noted that the pressure coefficient at the stagnation point is always positive which is consistent with the velocity measurements shown in [18] where the centerline velocity is always in the negative y-direction (negative wall-normal direction) even in the suction period.

Figure 5 shows the non-dimensional turbulent kinetic energy profiles at various streamwise positions. As can be seen, the turbulence kinetic energy levels decrease both in the inner-wall and outer-region of the wall-jet in the streamwise direction. Similar to impinging jets, such a monotonic (decreasing) profile for the turbulence kinetic energy leads to a monotonic Nu profile on the target plate where no off-the-stagnation secondary peaks are seen.

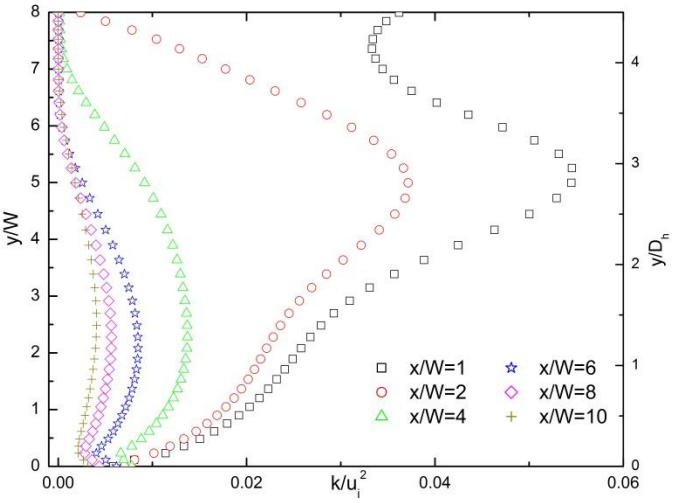

Figure 5 Non-dimensional turbulence kinetic energy profiles at various x/W for Re_j = 211 and H/D_h = 5 (H/W =8.89).

Figure 6 demonstrates the target plate Nu distribution. Peak heat transfer coefficient value is obtained at the stagnation point and is invariant with phase angle. Once the initial transients die,

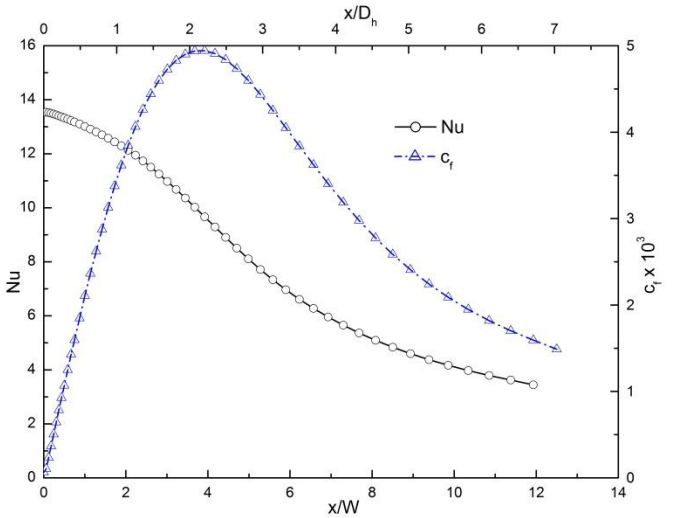

Figure 6 Nusselt number and skin friction factor profiles as a function of x/W for Re_j = 211 and H/D_h = 5 (H/W = 8.89).

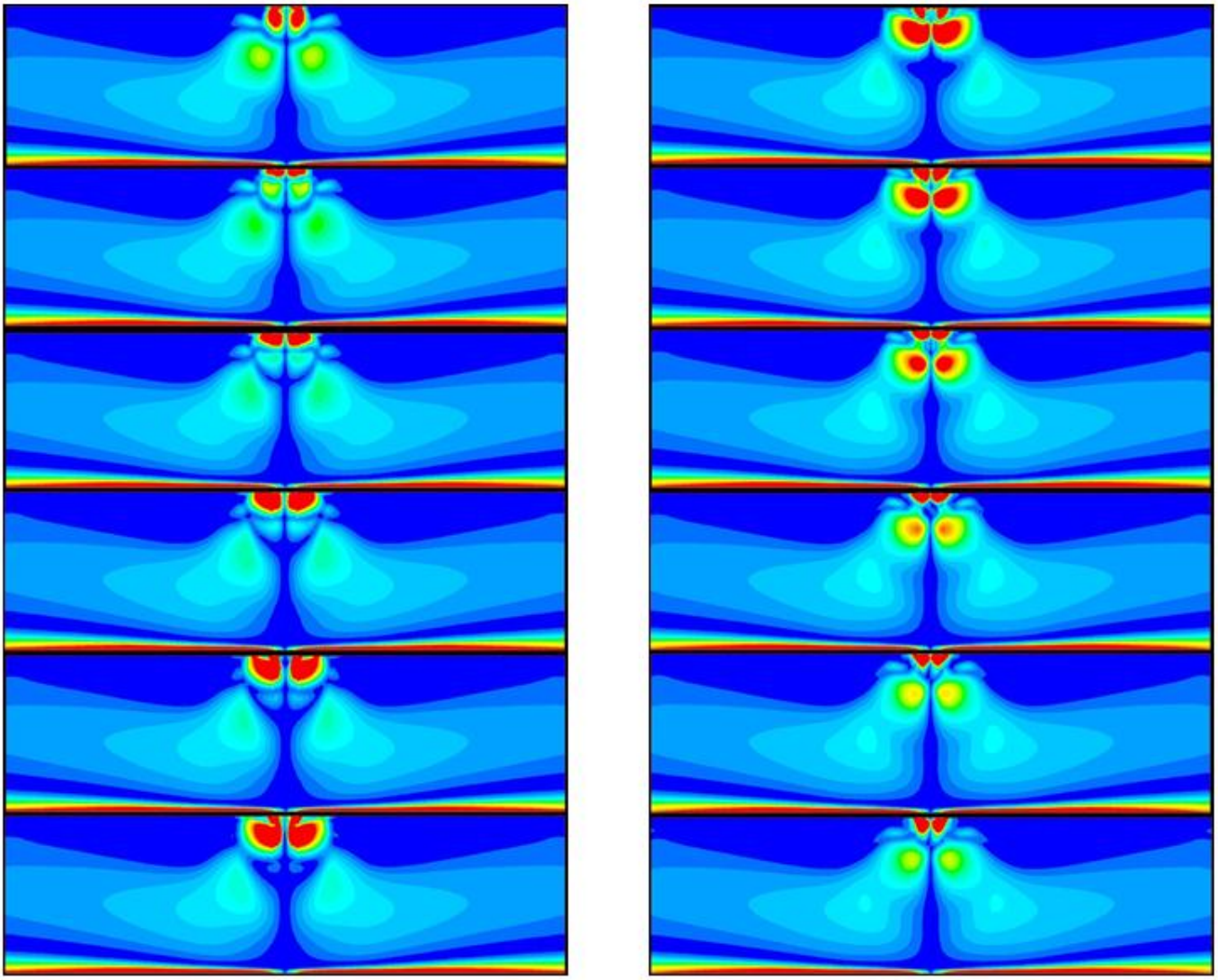

Figure 7 Vorticity contours during the injection and suction periods, t/ζ = 600, H/D_h = 5 (H/W = 8.89) and Re_j = 211.

two symmetric vortices (w.r.t. the stagnation line) emanated from the nozzle exit grow in size with the entrainment from the surrounding fluid, however they don't reach or approach close enough onto the target plate that they have no effect on the *Nu* or minimal effect on the skin friction distribution of the surface. The skin friction peak changes about 10% in a cycle, however, qualitatively, the shape of the distribution does not change, i.e. it has its minimum at the stagnation point and a single maximum at $x/W \approx 4$. Note that this is also consistent with the half-width of the pressure distribution similar to the orthogonal jet impingement behavior.

Vortices are spinning, often turbulent, flow of fluid in a region. The speed and rate of rotation of the fluid in a free (irrotational) vortex are the greatest at the center, and decrease progressively with distance from the center, whereas the speed of a forced (rotational) vortex is zero at the center and increases proportional to the distance from the center. Both types of vortices exhibit a pressure minimum at the center, though the pressure minimum in a free vortex is much lower. Synthetic jets' cooling performance relies on vortex generation and the behavior of vortices over the cooled surface. The next paragraph will discuss the vortex structures determined at the injection and suction periods by the present CFD analysis.

Figure 7 shows the vorticity contours in a full period starting at t/ζ =600 and at the dimensionless nozzle-to-plate distance of 5 (H/D_h = 5) for Re_j = 211. As can be seen, the vortex pair emanated from the nozzle exit at a point, at which the maximum velocity of the injection period is obtained (φ=90°), is still attached to the nozzle however it grows in size and strength until the early suction period. Following its detachment, the strength of the vortex pair attenuates, nevertheless it keeps growing in size. When the injection period begins, the existing vortex pair is reattached to the new vortex pair emanated from the nozzle. As mentioned earlier, this

vortex pair does not reach in the close proximity of the target surface around the stagnation area or affect the wall jet, therefore does not increase the momentum transport towards the wall to enhance the target plate surface heat transfer profiles.

CONCLUSIONS

This paper presents a computational study that has been performed for a meso-scale synthetic jet driven by a sine wave. Boundary conditions in the computational study have been taken from the previous experimental work [18] to determine the target plate surface profiles and the vortex field. Based on the present numerical results, the following conclusions are drawn:

- Pressure distribution on the target plate is of Gaussian shape if there are no sub-ambient pressure values. The synthetic jet has a considerably higher half-width than that of its impinging jet counterpart.
- Skin friction and heat transfer coefficient profiles on the target plate do not exhibit any secondary peaks at the given Re_j and nozzle-to-plate distance. Consistently, the turbulence kinetic energy profiles at various streamwise distances show that the turbulence levels decrease monotonically in the inner-wall and outer-wall regions of the wall-jet region.
- As expected, with no secondary peaks on the heat transfer coefficient distribution, the peak *Nu* is obtained at the stagnation point. In addition, the *Nu* distribution is invariant with the phase angle, i.e. not time dependent for $t/\zeta \geq 600$.
- Similarly, skin friction factor reaches its peak value at $x/W \approx 4$ and monotonically decreases thereafter. The streamwise location for the skin friction factor peak is consistent with the half-width of the pressure profiles.
- The vortex pairs emanated from the nozzle-exit seems to have no effect on the momentum transport towards the wall and, consequently, the surface profiles.

REFERENCES

[1] Petroski, J., Arik, M., and Gursoy, M., Piezoelectric Fans: Heat Transfer Enhancements or Electronics Cooling, *ASME-JSME Thermal Engineering and Summer Heat Transfer Conference 2008*, HT-2008-56405, Jacksonville, FL, August, 2008.

[2] Acikalin, T., Sauciuc, I., and Garimella, S. V., Piezoelectric Actuators for Low-Form-Factor Electronics Cooling, *The ASME/Pacific Rim Technical Conference and Exhibition on Integration and Packaging of Micro, Nano, and Electronic Systems (InterPACK '05)*, IPACK2005-73288, San Francisco, CA, July, 2005.

[3] Go, D., Garimella, S.V, Fisher, T., and Mongia, R., Ionic Winds for Locally Enhanced Cooling, *Journal of Applied Physics*, Vol. 102, 2007, 053302.

[4] Arik, M. Local heat transfer coefficients of a high frequency synthetic jets during impingement cooling over flat surfaces, *Heat Transfer Engineering*, Vol. 29(9), 2008, 763 – 773.

[5] Mittal, R., and Rampunggoon, P., On virtual aero-shaping effect of synthetic jets, *Phys. Fluids*, Vol. 14(4), 2002, 1533-1536.

[6] Lee, C. Y., and Glodstein, D. B., DNS of micro jets for turbulent boundary layer control, *AIAA 39th Aerospace Sciences Meeting and Exhibition*, AIAA 2001-1013, Reno, NV, January, 2001.

[7] Garg, J., Arik, M., Weaver, S., and Saddoughi, S., Micro fluidic jets for thermal management of electronics, *ASME Heat Transfer/Fluids Engineering Summer Conference*, FED F-346, Charlotte, NC, July, 2004.

[8] Erbas, N., Koklu, M., and Baysal, O., Synthetic jets for thermal management of microelectronic chips, *Proceedings of ASME IMECE 2005*, IMECE 2005-81419, Orlando, FL, 2005.

[9] Arik, M., Petroski, J., Bar-Cohen, A. and Demiroglu, M., Energy Efficiency of Low Form Factor Cooling Devices, *ASME International Mechanical Engineering Congress and Exposition*, IMECE2007-41275, Seattle, WA, November, 2007.

[10] Gutmark, E., Yassour, Y., and Wolfshtein, M., Acoustic enhancement of heat transfer in plane channels, *Proceedings of the Seventh International Heat Transfer Conference*, Munich, Germany, September, 1982, pp. 441-445.

[11] Yassour, Y., Stricker, J., and Wolfshtein, M., Heat transfer from a pulsating jet, *Proceedings of the Eighth International Conference*, San Francisco, CA, August, 1986, Vol. 3, pp. 1183-1186.

[12] Minichiello, A. L., Hartley, J. G., Glezer, A., and Black, W. Z., Thermal management of sealed electronic enclosures using synthetic jet technology, *Advances in Electronic Packaging*, EEP (19-2), 1997, pp. 1809-1812.

[13] Utturkar, Y., Arik, M., and Gursoy, M., An experimental and computational sensitivity analysis of synthetic jet cooling performance, *IMECE2006 ASME International Mechanical Engineering Congress and Exposition*, IMECE2006-13743, Chicago, IL, November, 2006.

[14] Garg, J., Arik, M., Weaver, S., Wetzel, T., and Saddoughi, S., Advanced localized air cooling with synthetic jets, *ASME Journal of Electronic Packaging*, Vol. 127, 2005, pp. 503-511.

[15] Arik, M., Utturkar, Y., and Gursoy, M., Interaction of Synthetic Jet Cooling Performance with Gravity and Buoyancy driven flows", *ASME InterPACK '07*, Vancouver, British Columbia, Canada, July, 2007.

[16] Seeley, C. E., Arik, M., Hedeen, R., Utturkar, Y., Wetzel, T. and Shih, M., Coupled acoustic and heat transfer modeling of a synthetic jet, *47th AIAA/ASME/ASCE/AHS/ASC Structures, Structural Dynamics and Materials Conference*, Newport, RI, May, 2006, pp. 1-13.

[17] Arik, M., An investigation into feasibility of impingement heat transfer and acoustic abatement of meso scale synthetic jets, *Journal of Applied Thermal Engineering*, Vol. 27(8-9), 2007, pp. 1483-1494.

[18] Arik, M., Sharma, R., Lustbader, J. and He, X., Comparison of synthetic and steady air jets for impingment heat transfer over vertical surfaces, *Intersociety Conference on Thermal and Thermomechanical Phenomena in Electronic Systems (ITHERM)*, San Diego, CA, May, 2012.